

IMPACT OF THE REVISED ANSI STANDARD ON ACCREDITED THERMOLUMINESCENCE DOSEMETER PROCESSORS

J. R. Cassata†, D. A. Schauer‡, M. E. Nelson†, G. A. Pertmer§ and G. K. Riel||

†United States Naval Academy, Engineering and Weapons Division
Rickover Bldg. 590 Holloway Rd, Annapolis, MD 21402-5042, USA

‡Science Advisor Naval Dosimetry Center

Navy Environment Health Center Detachment, Bethesda, MD 20889-5614, USA

§Department of Nuclear Engineering, University of Maryland at College Park
College Park, MD 20742-2115, USA

||Naval Surface Warfare Center Carderock Division
NSWCCD Code 682, Silver Spring, MD 20903-5640, USA

Received January 29 1996, Revised May 9 1996, Accepted June 4 1996

Abstract — Recent changes in ANSI N13:11 (1993) will have an impact on the performance of thermoluminescence dosimetry algorithms used to determine dose equivalent measurements. Accredited processors should update their algorithms to account for these changes. This paper quantifies the performance impact from the addition of beam codes M60 and H150, changes in C_K , and testing at angles. A predictive model that will determine new correction factors used in the calculation of dose equivalent is presented. A comparative study between predicted and experimental values is made and the validity of this approach is demonstrated with a proficiency test using the predicted values on a set of dosimeters irradiated at Pacific Northwest National Laboratory (PNNL). Extensive angular testing was also done at the National Institute of Standards and Technology (NIST) and is reported.

INTRODUCTION

Nuclear Regulatory Commission (NRC) regulations require processors of personnel dosimeters to be accredited by the National Voluntary Accreditation Program (NVLAP) annually with proficiency testing every two years⁽¹⁾. NVLAP proficiency testing was conducted against the American National Standard N13.11-1983⁽²⁾. In November of 1994, a memorandum was sent to all NVLAP Ionizing Radiation Dosimetry Program participants containing an advance copy of the Federal Register Notice (FRN) informing the public of a change in NVLAP proficiency testing^(3,4). Significant changes include: (1) Changes in the 'energy averaged air kerma to dose equivalent conversion factors' ($\bar{C}_{K,d,i}$) ranging from -9% to +13%⁽⁵⁾. (The subscripts used in this paper are defined as: K = air kerma, d = deep dose equivalent, s = shallow dose equivalent, i field type, and numbers 1 to 4 describe the chip position on the badge.) (2) Additional proficiency testing in beam codes M60 and H150. (3) Additional proficiency testing for angular irradiations from 0° to ±60° for vertical and horizontal orientations.

The purpose of this paper is to: (1) Quantify the impact of these changes on dosimetry processors. (2) Provide a predictive model that will allow processors to use their current correction factors ($C(H_d)$) to determine new $C(H_d)$ values with a comparative study between predicted and experimental $C(H_d)$ values. (3) Demonstrate the validity of this approach with dosimetry performance testing on irradiations done by the Pacific

Northwest National Laboratory (PNNL). (4) Report angular results for irradiations done at the National Institute of Standards and Technology (NIST).

MATERIALS, METHODS AND THEORY

Device used

The dosimeter used in this research was the Harshaw 8802 currently used by many research facilities, hospitals, and naval facilities in the United States. As shown in Figure 1, it contains four solid thermoluminescent (TL) chips that are all thin 0.3 cm squares with thicknesses of 0.015 inches for chips 1, 2, 4 and 0.006 inches for chip 3. Chips 1, 2, 3 are TLD-700 and chip 4 is TLD-600. TLD-700 is composed of 99.993% ⁷Li and TLD-600 is composed of 95.62% ⁶Li with a high neutron capture cross section (data supplied by the Harshaw Bicon Corporation). All chips are doped with Mg-Ti. The four chips are positioned at the four corners of a 3 × 4 cm rectangle between two clear 0.006 cm thick Teflon sheets. The Teflon/chip composite is mounted between two aluminium plates with four circular holes to accommodate the four chips. The aluminium card is placed in a plastic holder that is worn on a belt or clipped to a person's clothing. The holder is ABS plastic with various filters over each chip. Over the position for chips 1 and 4 there is a filtration of ABS plastic equal to 600 mg.cm⁻². Over the position for chip 2 there is 91 mg.cm⁻² of copper and 242 mg.cm⁻² of ABS plastic for a total of 333 mg.cm⁻². Over the position for chip 3

there is a thin aluminised Mylar film of 17 mg.cm^{-2} . Filters act as attenuating media causing the output of each chip on a single card to differ for the same irradiating field. This serves the purpose of differentiating the type and energy of the irradiating field.

The badges are processed by a Harshaw 8800 reader that uses hot nitrogen gas to heat the TLD. Each chip on the badge is treated as a separate independent channel. Reader measurements of nanocoulombs are converted to an observed Cs equivalent deep dose equivalent (ODDE) by a reader calibration factor (RCF). A RCF is determined for each of the four chip positions for each batch of TLDs processed from a set of reader calibration cards. However, it has been historically shown that the RCF for each chip position varies very little over time.

Each chip may vary in light sensitivity due to differences in the size, shape, mass, chemical composition, and processing. To make each chip equal in sensitivity a unique 'element correction coefficient' (ECC) is applied to each chip on each badge.

For all irradiations the TLDs were mounted on a $30 \times 30 \times 15 \text{ cm}$ slab phantom made of polymethyl methacrylate (common names Plexiglas, Lucite, Perspex).

Irradiations performed

For experimental determination of $C(H_d)$ factors, irradiations were done on single sources, single sources mixed with ^{137}Cs in ratios of 1:3, 1:1, and 3:1, and angular fields at badge orientations of $\pm 40^\circ$ and $\pm 60^\circ$ in both the horizontal and vertical positions. The single sources included betas from ^{90}Sr , photons from ^{137}Cs , and photons from beam codes M30, M60, M100, M150, and H150. Angular fields included photons from ^{137}Cs and beam codes M100, M150, and H150. All irradiations were done at NIST over a 5 month period in accordance with the Health Physics Society ANSI N13.11 1993 standard⁽⁶⁾. No less than 15 dosimeters per category were used for a total of 1255 irradiations.

Angular irradiations were done by rotating the phantom through a vertical axis located on the centre of the front face of the phantom. Counter clockwise rotation, as viewed from the top looking down onto the phantom, is defined as positive. Chip positions for horizontal and vertical orientations are shown in Figure 2. For positive angles in the horizontal orientation chips 3 and 4 are farther away from the source while chips 1 and 2 are closer. For positive angles in the vertical orientation chips 2 and 3 are farther away while chips 1 and 4 are closer.

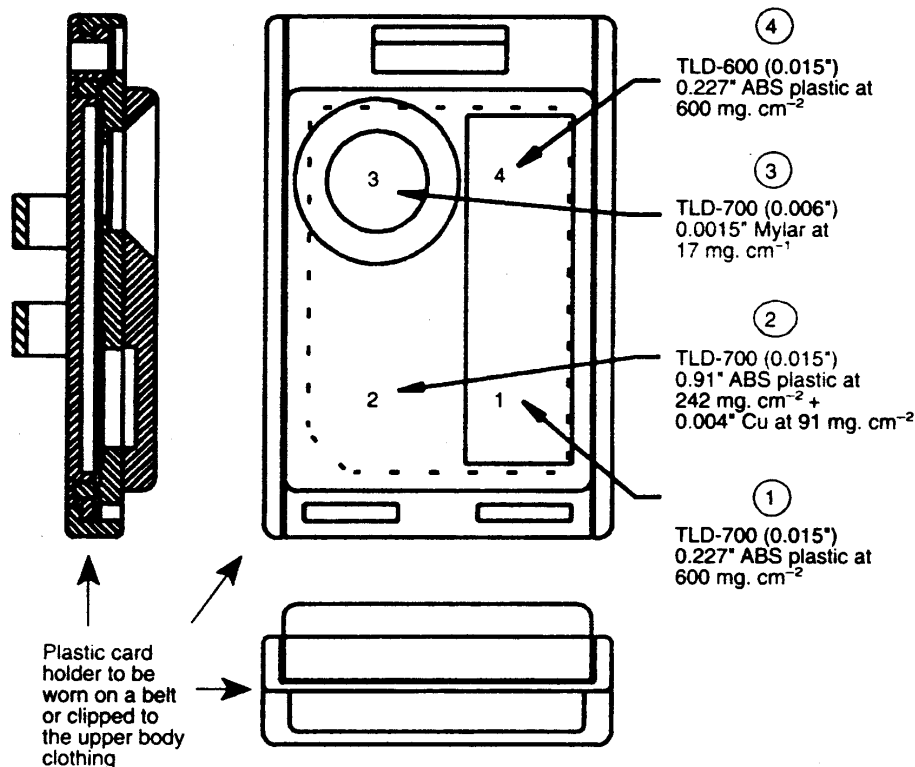


Figure 1. The 8802 four chip TLD card used for this research mounted in the plastic holder. The plastic holder contains the filters in front of each chip.

IMPACT OF ANSI STANDARD ON TLD PROCESSORS

The TLDs were annealed the morning of the irradiation and read within hours of completion. No more than a 12 h period occurred between annealing and reading. For this reason, pre-irradiation fade and post-irradiation fade were considered negligible. At least three control dosimeters were used each day to ensure that background radiation was negligible.

For dosimetry performance testing, 155 badges were irradiated at the PNNL. Currently used pre- and post-fade corrections were applied to those irradiations. Ten control dosimeters were used to determine the average background radiation. Five dosimeters were irradiated in each of the same single and mixed fields described above. No angular testing was done for the performance testing at PNNL.

THEORY

Fundamental concepts

The three most important quantities to be defined are the calculated deep dose equivalent (CDDE), the observed Cs equivalent deep dose equivalent (ODDE), and the expected deep dose equivalent (EDDE). Deep dose implies a tissue depth of 1 cm. Only deep dose terms and equations are mentioned in this paper to simplify the writing, but the analogous shallow dose terms and equations do exist. Shallow dose implies a tissue depth of 0.007 cm. To modify the equations for a shallow dose, the subscript 'd' would be replaced with an 's'.

The current TLD measurement system determines a

CDDE by multiplying a deep dose equivalent correction factor ($C(H_d)$) by an ODDE. The ODDE is the result of multiplying the measured light output (LO) by the ECC to account for individual chip sensitivity and then calibrating this product to ^{137}Cs equivalent dose equivalent value by dividing by a RCF. Equation 1 shows these relationships:

$$CDDE = C(H_d) ODDE = C(H_d) \frac{LO ECC}{RCF} \quad (1)$$

The $C(H_d)$ accounts for the fact that the TL material responds differently to different energies and types of radiation than it does to ^{137}Cs . $C(H_d)$ can be experimentally calculated by dividing the EDDE by the ODDE as shown by Equation 2.

$$C(H_d) = \frac{EDDE}{ODDE} \quad (2)$$

Once a $C(H_d)$ has been determined for each field, the algorithm determines the appropriate $C(H_d)$ for each measurement. The choice of which $C(H_d)$ to apply is typically based on ratios of measurements between the chips on a single badge. In general, better algorithms can be written with increasing numbers of chips on a single badge, provided that each chip has a different response to the measured field. Differences in response are obtained by placing filters over each chip or by using different TL materials in each chip. For the historical development and thorough understanding of the dose algorithm used, the reader is referred to References 7-12.

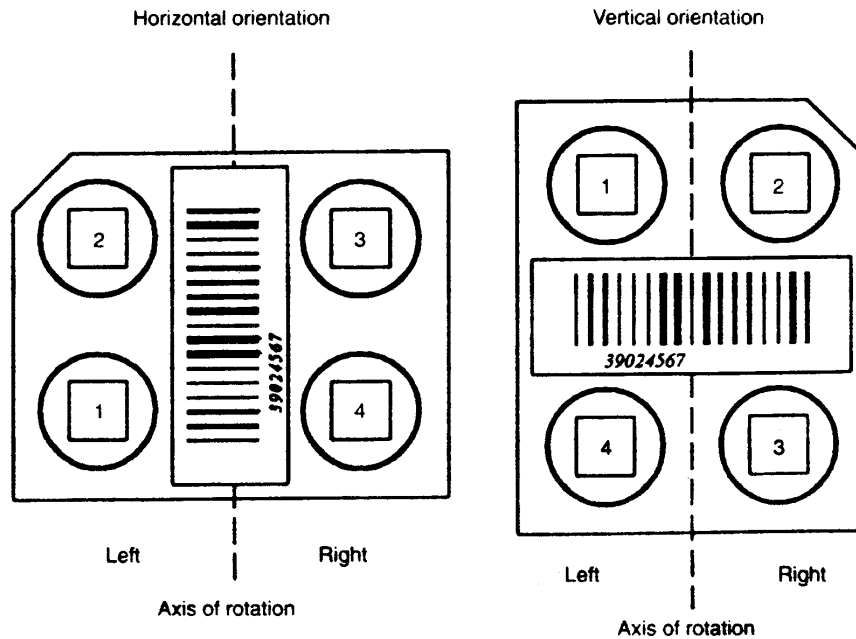


Figure 2. Diagram showing chip positions in the horizontal and vertical orientations for the angular irradiations. The irradiating beam would be perpendicular into the paper and the phantom would be behind the badges with the centre front face of the phantom on the axis of rotation shown.

The EDDE is the expected deep dose equivalent, in mSv, that a person would receive at a tissue depth of 1 cm if the person was standing in the radiation field being measured. When badges are irradiated in the laboratory, the EDDE is considered the 'truth' because the laboratory fields are well characterised, reproducible, and NIST traceable. For photons the EDDE for a single photon field 'i' is the product of $\bar{C}_{K,d,i}$ with the air kerma ($K_{a,i}$) as shown by Equation 3. The EDDE is not a function of light output from the TL material and is an independent quantity from the TLD measurement.

$$EDDE_i = \bar{C}_{K,d,i} K_{a,i} \quad (3)$$

The CDDE from the badge should ideally be equal in magnitude to the EDDE for a zero error measurement of dose equivalent. To measure how well a dosimetry system determines the EDDE the sum of the absolute bias ($|B|$) and standard deviation (S) is calculated for a statistically valid number of badges in each category tested. The sum of $|B|$ plus S is defined as the performance coefficient (PC) of the device. NVLAP criteria for passing each category is a 30% maximum $|B|$ or S and a 50% maximum PC⁽⁶⁾.

Derived equations

Equations in this section have been derived from first principles. As a practical matter only the results are presented here.

The TLD system discussed here uses a ¹³⁷Cs dose equivalent of 1.50 mSv as the calibration point. Changing the value of $C_{K,d,Cs}$ changes the RCF for each channel (see Appendix 1). For any channel the new RCF can be calculated from Equation 4. (All new and old values of C_K for all categories can be found in Reference 5.)

$$RCF_{new} = RCF_{old} \frac{C_{K,d,Cs,old}}{C_{K,d,Cs,new}} \quad (4)$$

The new $C(H_d)$ for any single field 'i' can be found from Equation 5:

$$\frac{C(H_d)_{i,new}}{C(H_d)_{i,old}} = \frac{ODDE_{i,old}}{ODDE_{i,new}} = \frac{\bar{C}_{K,d,i,new}}{\bar{C}_{K,d,i,old}} \frac{C_{K,d,Cs,old}}{C_{K,d,Cs,new}} \quad (5)$$

This equation allows the processor to update their existing single field correction factors without any new experimentation.

Photon equations in this paper have also been derived for beta exposures. For beta exposure $\bar{C}_{K,s,i}$ is not applicable. Beta equations can be written from the photon equations by setting the $\bar{C}_{K,s,i}$ term to 1. This is applicable to the shallow dose versions of Equations 5 and 9.

Mixed field irradiations used by NVLAP are ratios of ¹³⁷Cs with one of the X ray beams, ⁹⁰Sr, or moderated ²⁵²Cf. Modelling mixed radiation fields is based on superposition of each field. In the laboratory, a mixed field is really exposure to one field followed by another. Simultaneously irradiating a single TLD with two

sources is practically never done for logistical reasons and the effects of doing so are considered negligible. Usage in the field depends on superposition holding true since the dose is accumulated over a month or more.

New $C(H_d)$ factors for any mixed field can be determined from single field values using a simple weighted average as shown by Equation 6:

$$C(H_d)_{mix} = \left(\frac{1}{1+R} \right) C(H_d)_{Cs} + \left(\frac{R}{1+R} \right) C(H_d)_i \quad (6)$$

where R is defined as the ratio of $EDDE_i$ over $EDDE_{Cs}$. An alternative equation to predict mixed field $C(H_d)$ factors from single field factors is shown by Equation 7:

$$C(H_d)_{mix} = \frac{C(H_d)_i C(H_d)_{Cs} (1+R)}{R C(H_d)_{Cs} + C(H_d)_i} \quad (7)$$

The last two equations greatly reduce the need for performing experimental measurements to obtain the new correction factors, resulting in substantial savings of time and money to the processor.

As stated previously, algorithms must choose the correct $C(H_d)_i$ or $C(H_d)_{mix}$ based on some measurement or combination of measurements from the TLD badge. Traditionally, the ratio of light output from chip positions 1 over 2 has been the primary parameter used for the Harshaw 8802 TLD. Other TLD devices attempt to improve on this by using more chip position data so that more fundamental information may be obtained to make better decisions.

In order for the equations derived in this paper to be useful in updating existing algorithms, ratios of measurements from different chip positions must also be predicted. Equation 8 can be used for this prediction and it shows that the ratios between TL chips in a badge does not change with changes in $\bar{C}_{K,d,i}$. (Note: Additional numerical subscripts on each parameter are now necessary to distinguish each individual chip position on the badge.)

$$\frac{ODDE_{1,i}}{ODDE_{2,i}} = \frac{k_{1,i} k_{2,Cs}}{k_{2,i} k_{1,Cs}} \quad (8)$$

The lower case 'k' is a response constant that is experimentally determined with units of nanocoulombs per mGy. Equation 8 is an extremely important finding in the updating of existing algorithms. This means that for single radiation fields the ratio between any two chip positions will be unaffected by changes in $\bar{C}_{K,d,i}$. This is not the case for mixed fields.

For mixed fields the ratio of measurements between chip positions has been found to be function of $\bar{C}_{K,d,i}$ as shown by Equation 9:

$$\frac{ODDE_{1,mix}}{ODDE_{2,mix}} = \frac{\left(\frac{k_{1,i}}{k_{1,Cs}} R \frac{C_{K,d,Cs}}{\bar{C}_{K,d,i}} + 1 \right)}{\left(\frac{k_{1,i}}{k_{1,Cs}} R \frac{ODDE_{2,i}}{ODDE_{1,i}} \frac{C_{K,d,Cs}}{\bar{C}_{K,d,i}} + 1 \right)} \quad (9)$$

The lower case 'k' must be determined through

IMPACT OF ANSI STANDARD ON TLD PROCESSORS

experimental measurements for each single radiation source. However, estimates of chip ratios can be made by using a weighted average between each single source in the mixed field. For example, if the ratio of chip 1 over chip 2 for a single field of M60 is 1.661 and for a single field of ¹³⁷Cs is 1.000, then the ratio for a 3 to 1 mixture of M60 with ¹³⁷Cs is $0.75 \times 1.661 + 0.25 \times 1.000 = 1.496$. The actual experimentally determined ratio of chip 1 over 2 was 1.472 yielding a per cent difference of 1.6%.

Mixed field equations have been shown to be consistent with the single field equations at the extreme ratio values of all one source or the other. This is a necessary condition for a valid mixed field equation.

RESULTS

Tables 1 and 2 quantify four different courses of action that a processor can follow. (1) Do nothing and continue to use existing algorithms without making any changes (Row 1). (2) Use the equations in this paper along with existing C(H_d) and C(H_s) values to update

existing algorithms with no new experimentation necessary (Row 2). (3) Perform single field irradiations and use the equations in this paper to predict the mixed field data to update algorithms (Rows 3 and 4). (5) Do both single and mix field irradiations to experimentally determine all new correction factors for algorithms (Row 5).

Table 1 directly compares the values of the C(H_d) and C(H_s) correction factors from the method indicated with the experimentally determined values. This is a way of normalising all the data to those obtained experimentally.

Table 2 compares the results from applying each of the sets of C(H_d) and C(H_s) correction factors to a set of 155 dosimeters irradiated by the PNNL. The four quantities used for comparison purposes are the average per cent increase in the PC, the range in the B, the range in the S, and the range in the PC.

The numbers in Tables 1 and 2 represent average values from 25 categories comprised of single and mixed fields of Beams codes M30, M60, M100, M150, H150, ⁹⁰Sr, and ¹³⁷Cs. The mixed fields are mixtures of ¹³⁷Cs with the other fields in dose equivalent ratios of 3:1, 1:1, and 1:3.

Table 1. Summary of results comparing: (1) the average absolute per cent difference in C(H_s) and C(H_d) between the method listed and those obtained from doing all irradiations, and (2) the range of per cent differences in C(H_s) and C(H_d) between the method listed and those obtained from doing all irradiations. (Note: for Tables 1 and 2 the numbers represent average values from 25 categories comprised of single and mixed fields of Beams codes M30, M60, M100, M150, H150, ⁹⁰Sr, and ¹³⁷Cs).

Col (A)	Col (B)	Col (C)	Col (D)
Method		(1) Average absolute per cent difference in C(H _s). (2) Range of per cent differences in C(H _s). (Both per cent differences are between method indicated and doing all irradiations.)	(1) Average absolute percent difference in C(H _d). (2) Range of per cent differences in C(H _d). (Both per cent differences are between method indicated and doing all irradiations.)
Row 1	Using existing correction factors, no changes. (Requires 0 new irradiations.)	(1) 5.1% (2) -12.4% to +12.3%	(1) 6.5% (2) -13.2% to +11.9%
Row 2	Using Equations 5, 7, and existing correction factors to predict new correction factors. (Requires 0 new irradiations.)	(1) 4.5% (2) -11.2% to +5.6%	(1) 3.6% (2) -6.8% to +4.3%
Row 3	Making single field irradiations and Equation 6 to predict mixed field correction factors. (Requires 105 single field irradiations.)	(1) 2.9% (2) -11.7% to +4.9%	(1) 1.2% (2) -0.8% to +7.8%
Row 4	Making single field irradiations and Equation 7 to predict mixed field correction factors. (Requires 105 single field irradiations.)	(1) 3.0% (2) -11.8% to +0.7%	(1) 0.9% (2) -3.4% to +0.0%
Row 5	Making single field and mixed field irradiations. (Requires 375 irradiations with 2/3 involving mixed fields.)	(1) 0.0% (2) -0.0% to +0.0%	(1) 0.0% (2) -0.0% to +0.0%

Tables 3 and 4 show the normalised results for angular irradiations of beam code M100. Beams codes M150, H150, and ¹³⁷Cs were also done. Tables 3 and 4 are essentially two halves of one larger table as indicated by the continuous labeling of the columns A through M.

Tables 5, 6, and 7 are summaries of all beam codes tested at angles. These tables summarise the important changes that occur with the angle of irradiation.

CONCLUSIONS

Table 1 shows that using existing C(H_j) correction factors results in the largest per cent differences of all the methods shown and a processor could expect per cent errors commensurate with the magnitude changes that occur in the $\bar{C}_{K,d,i}$ factors. In the new ANSI standard $\bar{C}_{K,d,i}$ changed by an average absolute per cent difference of 5.5%, with a range in per cent difference of -9 to +13%. These numbers are nearly identical in magnitude to the numbers shown in row 1 of Table 1. This gives the processor an overall perspective on the impact

of the present and future changes in the $\bar{C}_{K,d,i}$ conversion factors on existing correction factors.

The values in Table 2 could be considered a better basis for comparison than Table 1 since each processor is being tested in the B, S, and PC of their systems and not in the values of C(H_j) and C(H_i).

Row 1 of Table 2 shows the need to update existing algorithms because of the increase in PC and B. Application of the existing correction coefficients to validation data from PNNL results in a 3 to 5% increase in the average PC with a maximum bias of 24.8%, dangerously close to the NVLAP accreditation bias limit of 30%.

Row 2 in Tables 1 and 2 shows that the resulting errors from using existing C(H_d) values can be significantly reduced by using Equations 5 and 7 to predict new C(H_d) values from the existing ones. Increases in PC dropped about 30% for shallow and 70% for deep with about a 50% drop in bias for both shallow and deep. Since no new experimentation is necessary, this route requires very little time or cost expenditure and should be done at a minimum.

Table 2. Summary of results listing: (1) the average per cent increase in the performance coefficient (PC), (2) the range of bias (B), (3) the range of standard deviation (S), and (4) the range in PC; for deep and shallow measurements. Note that the increase in PC is calculated by subtracting PC_a from PC_b, where PC_a is the average PC obtained by applying the C(H_j) and C(H_d) values from the method indicated to the PNNL data. PC_b is the average PC obtained by applying the experimentally determined C(H_j) and C(H_d) values to the PNNL data.

Col (A)	Col (B)	Col (C)	Col (D)
Method		(1) Average per cent increase in the shallow PC by using method indicated. (2) Range in B. (3) Range in S. (4) Range in the shallow PC.	(1) Average per cent increase in the deep PC by using method indicated. (2) Range in B _d . (3) Range in S _d . (4) Range in the Deep PC.
Row 1 Using existing correction factors, no changes. (Requires 0 new irradiations.)		(1) 3.1% (2) -14.9% ≤ B ≤ 24.8% (3) 1.1% ≤ S ≤ 6.6% (4) 3.2% ≤ PC ≤ 27.1%	(1) 5.5% (2) -17.0% ≤ B ≤ 14.1% (3) 0.7% ≤ S ≤ 5.8% (4) 3.6% ≤ PC ≤ 20.0%
Row 2 Using Equations 5, 7, and existing correction factors to predict new correction factors. (Requires 0 new irradiations.)		(1) 2.4% (2) -12.6% ≤ B ≤ 1.9% (3) 1.1% ≤ S ≤ 5.7% (4) 3.3% ≤ PC ≤ 17.5%	(1) 1.8% (2) -12.5% ≤ B ≤ 5.4% (3) 0.8% ≤ S ≤ 5.2% (4) 2.1% ≤ PC ≤ 16.6%
Row 3 Making single field irradiations and Equation 6 to predict mixed field correction factors. (Requires 105 single field irradiations.)		(1) 0.6% (2) -16.0% ≤ B ≤ 2.9% (3) 1.1% ≤ S ≤ 5.9% (4) 2.0% ≤ PC ≤ 19.9%	(1) 0.2% (2) -16.1% ≤ B ≤ 5.4% (3) 0.8% ≤ S ≤ 5.1% (4) 1.7% ≤ PC ≤ 19.3%
Row 4 Making single field irradiations and Equation 7 to predict mixed field correction factors. (Requires 105 single field irradiations.)		(1) 1.2% (2) -15.8% ≤ B ≤ 1.9% (3) 1.1% ≤ S ≤ 5.9% (4) 2.1% ≤ PC ≤ 19.0%	(1) 0.2% (2) -16.1% ≤ B ≤ 5.4% (3) 0.8% ≤ S ≤ 5.1% (4) 1.7% ≤ PC ≤ 19.3%
Row 5 Making single field and mixed field irradiations. (Requires 375 irradiations with 2/3 involving mixed fields.)		(1) 0.0% (2) -16.0% ≤ B ≤ 1.9% (3) 1.1% ≤ S ≤ 5.9% (4) 2.5% ≤ PC ≤ 19.0%	(1) 0.0% (2) -16.1% ≤ B ≤ 6.3% (3) 0.8% ≤ S ≤ 5.1% (4) 1.3% ≤ PC ≤ 19.3%

IMPACT OF ANSI STANDARD ON TLD PROCESSORS

Table 3. Summary of results showing the per cent change in chip response with angle of irradiation for beam code M100. Values at each angle are normalised to the measurement at 0°. The subscripts on ODDE refer to the chip position on the badge.

Col (A)	Col (B)	Col (C)	Col (D)	Col (E)	Col (F)
Beam code M100 H = Horizontal V = Vertical	% decrease in ODDE ₁ per mGy of air kerma received as compared to 0° measurement	% decrease in ODDE ₂ per mGy of air kerma received as compared to 0° measurement	% decrease in ODDE ₃ per mGy of air kerma received as compared to 0° measurement	% decrease in ODDE ₄ per mGy of air kerma received as compared to 0° measurement	Value of $\bar{C}_{m,d,m100}$ received as compared (mSv/mGy) to 0° measurement
Row 1 -60° H	20.00	27.00	15.00	12.73	1.14
Row 2 -40° H	9.63	9.73	3.96	3.53	1.39
Row 3 0°	0.00	0.00	0.00	0.00	1.52
Row 4 +40° H	7.79	6.41	4.78	6.20	1.39
Row 5 +60° H	14.12	21.43	19.66	16.66	1.14
Row 6 -60° V	19.49	21.95	15.24	11.23	1.14
Row 7 -40° V	10.72	8.77	5.61	4.76	1.39
Row 8 0°	0.00	0.00	0.00	0.00	1.52
Row 9 +40° V	8.94	9.99	6.46	4.41	1.39
Row 10 +60° V	14.43	25.66	19.73	10.75	1.14

Table 4. Summary of results showing the variation in C(H_d) and ODDE₁/ODDE₂ ratio from irradiating TLDs at various angles for beam code M100. Values at each angle are normalised to the measurement at 0°. The subscripts on EDDE and ODDE refer to the chip position on the badge.

Col (G)	Col (H)	Col (I)	Col (J)	Col (K)	Col (L)	Col (M)
Beam code M100 H = Horizontal V = Vertical	% decrease in $\bar{C}_{k,d,m100}$ compared to 0° value	% increase in exposure time to achieve a constant EDDE ₁ based on the decreasing C _k value in Col (H)	% increase in exposure time to achieve a constant ODDE ₁ based on the decreasing Chip 1 value in Col (B)	% increase in C(H _d) Chip 1 as compared to 0° value. (Negatives imply decrease)	% increase in ODDE ₁ /ODDE ₂ ratio as compared to 0° value. (Negatives imply decrease)	Number of standard deviations that the ODDE ₁ / ODDE ₂ ratio is from the mean ODDE ₁ /ODDE ₂ ratio at 0°
Row 1 -60° H	25.00	33.33	25.00	-6.51	9.58	3.04
Row 2 -40° H	8.55	9.35	10.66	0.99	0.10	0.03
Row 3 0°	0.00	0.00	0.00	0.00	0.00	0.00
Row 4 +40° H	8.55	9.35	8.45	-1.11	-1.48	0.47
Row 5 +60° H	25.00	33.33	16.44	-12.83	9.31	2.95
Row 6 -60° V	25.00	33.33	24.20	-7.07	3.15	1.00
Row 7 -40° V	8.55	9.35	12.01	2.20	-2.14	0.68
Row 8 0°	0.00	0.00	0.00	0.00	0.00	0.00
Row 9 +40° V	8.55	9.35	9.81	0.17	1.17	0.37
Row 10 +60° V	25.00	33.33	16.86	-12.56	15.10	4.79

Table 5. Summary of ranges in chip response with angle of irradiation for M100, M150, H150 and ¹³⁷Cs. Negative values indicate decreases in response as compared to 0° measurements while positive values indicate increases in response. Values from all four chip positions are considered in each range.

Angle	M100 (average energy 51 keV) Range of normalised response	M150 (average energy 70 keV) Range of normalised response	H150 (average energy 117 keV) Range of normalized response	¹³⁷ Cs (Average energy 662 keV) Range of normalised response
±40°	-10% to -4%	-8% to -1%	-5% to +3%	-4% to +5%
±60°	-27% to -15%	-19% to -10%	-12% to -2%	-5% to +10%

In the absence of existing correction coefficients the predictive model based on single field irradiations must be used. These results are shown in Rows 3 and 4 in Tables 1 and 2. The results shown in Rows 3 and 4 rival the results from doing all the experimental irradiations under the new $\bar{C}_{K,d,i}$ values. This shows that all mixed field data can accurately be predicted from single field data in the non-accident dose ranges. This represents an extremely significant finding reducing by two thirds the number of experimental irradiations and removing the need to perform mixed field irradiations. Irradiating a TLD in a mixed field involves using two consecutive sources, a procedure both laborious and costly.

Standard deviations for all methods shown in Table 2, were in the same range of 1 to 6%. This allows a conservative estimate to be made on the magnitude of the standard deviation. This is a valuable piece of information when assessing a dosimetry system. For example, the minimum PC can be estimated if the bias is known by other estimates. Table 6 lists the increase in bias that results from using the $C(H_d)$ values at 0° for other angles of irradiation. An estimation of the PC can be made by adding a 6% standard deviation to any value in the table.

Evaluating the changes in chip response that occur with angle of irradiation is difficult because there are several phenomena changing simultaneously. Physical changes that occur from badge rotation include: (1) shielding effects of the filters over each chip; (2) scattering effects from the TLD case and phantom; and (3) distances from the source to each chip.

Table 3 shows a measurable variation in response due to the changes in source to chip distances that occur as the badge is rotated. As the badge is rotated through

positive angles in the horizontal orientation, chips 1 and 2 move closer to the source while chips 3 and 4 move farther away. The opposite is true for rotation through negative angles (refer to Figure 1). Using the inverse square law, the response for chips 1 and 2 at $+60^\circ$ should be about 2% larger than at -60° and 1.5% larger at $+40^\circ$ than at -40° . The numbers in Table 3 qualitatively show these trends. However, the change in response between plus and minus 40° or 60° is about double in magnitude that predicted by the inverse square law. No explanation is offered for this observation. The same analysis applies to the vertical orientation yielding similar results.

Changes in response of the TL material with the angle of irradiation become more of an issue for lower energy sources. Table 3 shows that for beam code M100 at rotations of $\pm 40^\circ$, the chip response decreases about 4 to 10% and at $\pm 60^\circ$ it decreases about 15 to 27%. The decrease in chip response with angle lessens in magnitude with increasing energy of the beam as shown by Table 5.

The data show that $C(H_d)$ is a function of irradiating angle but this is only a significant factor at $\pm 60^\circ$ irradiations. Table 4 shows that the decrease in the dose equivalent that results with increasing angle occurs at a different rate than the decrease in chip response. This means that the EDDE and ODDE change at different rates, thus causing the $C(H_d)$ to be a function of angle (see Equation 2). Irradiations at $\pm 40^\circ$ can be treated as if they were at 0° with no significant increase in bias. However, Table 6 shows that up to a 12.8% increase in the bias can occur by using the $0^\circ C(H_d)$ factors for $\pm 60^\circ$ irradiations.

Equally important to the changes in $C(H_d)$ that occur

Table 6. Summary of ranges in bias if the $0^\circ C(H_d)$ factor is used for the listed angles.

Angle	M100 range in bias	M150 range in bias	H150 range in bias	^{137}Cs range in bias
$\pm 40^\circ$	-1.1% to +2.2%	-3.4% to +0.9%	-3.8% to -0.8%	-0.8% to +1.4%
$\pm 60^\circ$	-12.8% to -6.5%	-10.6% to -2.9%	-11.6% to -7.2%	-5.8% to -1.9%

Table 7. Summary of the range in the number of standard deviations that the $\text{ODDE}_1/\text{ODDE}_2$ ratio is from the mean $\text{ODDE}_1/\text{ODDE}_2$ ratio at 0° for beam codes M100, M150, H150, ^{137}Cs .

Angle	M100 Range in the number of standard deviations that the $\text{ODDE}_1/\text{ODDE}_2$ ratio is from the mean $\text{ODDE}_1/\text{ODDE}_2$ ratio at 0°	M150 Range in the number of standard deviations that the $\text{ODDE}_1/\text{ODDE}_2$ ratio is from the mean $\text{ODDE}_1/\text{ODDE}_2$ ratio at 0°	H150 Range in the number of standard deviations that the $\text{ODDE}_1/\text{ODDE}_2$ ratio is from the mean $\text{ODDE}_1/\text{ODDE}_2$ ratio at 0°	^{137}Cs Range in the number of standard deviations that the $\text{ODDE}_1/\text{ODDE}_2$ ratio is from the mean $\text{ODDE}_1/\text{ODDE}_2$ ratio at 0°
$\pm 40^\circ$	0 to 0.7	0.1 to 0.8	0.4 to 1.1	1.4 to 2.6
$\pm 60^\circ$	1 to 4.8	1 to 1.8	0 to 1.7	2.3 to 2.9

with irradiation angle are the changes in the ratios of chip responses. Table 7 shows how the ratio of $ODDE_1$ over $ODDE_2$ changes with irradiation angle. The ranges shown are in units of the number of standard deviations the listed angular ratio is from the mean ratio at 0° . Algorithms developed by the Naval Dosimetry Center use the value of one standard deviation from the mean value as a numerical boundary in their algorithms.

Table 7 shows that ratios at $\pm 40^\circ$ for beam codes M100, M150, and H150 are within one standard deviation so there is no way to discriminate these irradiations from irradiations at 0° . In fact, this is good since the $C(H_d)$ correction factors at $\pm 40^\circ$ were essentially the same as those at 0° , removing the need for discrimination between irradiations at these angles. Irradiating with M100, M150, and ^{137}Cs at $\pm 60^\circ$, yield ratios with greater than one standard deviation so that it may be possible to have an algorithm apply a more exact correction factor. If the processor decides to treat these angular irradiations as if they were the same beam codes at 0° , incorrect values of $C(H_d)$ will be applied, resulting in a range of additional bias of 1.9 to 12.8%.

Three of the four ratios for H150 at $\pm 60^\circ$ are less than one standard deviation from the mean value at 0° , making it impossible for an algorithm to discriminate between them. This will result in an additional bias of 7.3 to 11.6% using existing algorithm techniques.

The additional bias discussed in the previous two paragraphs assumes that the algorithm will be able to determine the correct beam code, a separate concept from the discussion of determining the correct angle of irradiation for that beam code. The magnitude of chip ratios for ^{137}Cs irradiations at $\pm 60^\circ$ are the same as those for H150 at 0° . The correction factors differ over 20% between them, meaning that the processor has the possibility of an additional increase in bias by this amount. In this case, it is necessary to choose a correction factor in the middle of the range between these correction factors. Using a mid-range value results in an additional bias of 10% all the time. This should not put the processor over the 30% limit in the NVLAP proficiency criteria. However, having an additional 0% half of the time and 20% the other half of the time, leaves the processor more susceptible to exceeding NVLAP limits.

The overall conclusion for angular irradiations is that significant measurement errors will occur at $\pm 60^\circ$ irradiations. Processors using existing devices need to do irradiations at $\pm 60^\circ$ and include these data in the design of their measurement systems. Over-fitting the data is worse than using mid-range compromises when different categories of irradiation cannot be differentiated from each other. New devices need to account for the effects of rotating dosimeters in low and high energy fields. Filters may need to be designed so that their half-value thickness changes with rotation. Averaging redundant chip measurements on a single badge may become necessary and chip shapes may need to be more curved than flat.

Current devices are close to their maximum capabilities. As NVLAP proficiency criteria becomes more restrictive, new materials, better designs, and more sophisticated algorithm techniques will be needed to keep pace.

ACKNOWLEDGEMENTS

The authors wish to thank Edward Boswell, Paul Lamperti, and Chris Soares from the National Institute of Standards and Technology for their assistance with the radiation sources. This work was supported by the Naval Dosimetry Center, Naval Surface Warfare Center Carderock Division, and Naval Sea Systems Command 04R. The views expressed in this article are those of the authors and do not reflect the official policy or position of the US Navy or any other organisation associated with this research.

APPENDIX 1

The purpose of this appendix is to show why a change in $C_{K,d,Cs}$ results in a change in the RCF for the dose algorithm used by the United States Navy. This analysis assumes nothing else changes in the physical devices used to irradiate and read the TLD cards.

The TLD system discussed here is the one used by the United States Navy to process their TLDs. It uses a NIST traceable local ^{137}Cs source at a dose equivalent of 1.50 mSv as the calibration point. The value of $C_{K,d,Cs}$ increased from 1.17 to 1.21 in the new NVLAP testing criteria. For any channel the RCF is calculated by Equation A1.

$$RCF = \frac{\frac{1}{N} \sum_{w=1}^N (\text{Light output in nanocoulombs from Cs exposure})_w (ECC)_w}{EDDE \text{ in mrem from the Cs exposure in 6610}} \quad (A1)$$

Substitution of Equation 3 into A1 yields Equation A2

$$RCF = \frac{\frac{1}{N} \sum_{w=1}^N (LO_w ECC_w)}{C_{K,d,Cs} K_{a,Cs}} \quad (A2)$$

The numerator of Equation 10 is just the average value of the adjusted light output and can be expressed in terms of the field causing the response by introducing a proportionality constant ' k_C ' as shown in Equation A3.

$$LO ECC = k_C K_{a,Cs} \quad (A3)$$

where k_C is the proportionally constant that converts the total air kerma of the ^{137}Cs field to nanocoulombs of light output in the reader. The units on this constant

are nonocoulombs per mGy. This constant assumes the TLD has a linear response with dose. It is a function of the type of radiation, the energy of the radiation, and the half-value thickness of the material in front of the TL chip.

Substitution of Equation A3 into Equation A2 yields Equation A4:

$$RCF = \frac{k_{Cs}}{C_{K,d,Cs}} \quad (A4)$$

Taking a ratio of Equation A4 eliminates the need to solve for the constant and results in Equation 4 (shown again for convenience):

$$RCF_{new} = RCF_{old} \frac{C_{K,d,Cs,old}}{C_{K,d,Cs,new}} \quad (4)$$

Equation 4 shows that a linear increase in $C_{K,d,Cs}$ results in a hyperbolic decrease in the RCF. Equation 4 can also be expressed in terms of per cent change by Equation A5. Here the negative sign indicates that the RCF decreases with an increase in $C_{K,d,Cs}$:

$$Y\% \text{ change in RCF} = \frac{(-100)(X\% \text{ change in } C_{K,d,Cs})}{100 + X\% \text{ change in } C_{K,d,Cs}} \quad (A5)$$

A comparative analysis between the changes predicted by Equation 4 and the experimental data is summarized in Table A1.

Physical understanding of the relationship between $C_{K,d,Cs}$ and the RCF can be explained as follows. (The explanation will first be built on the assumption that the calibration TLDs are exposed directly at NIST. Later it will be shown that using a NIST traceable local source to irradiate the calibration TLDs does not change the result of the analysis).

To obtain the denominator of Equation A1 the calibration cards are exposed to 1.5 mSv of ^{137}Cs at NIST. Equation A6 shows that as $C_{K,d,Cs}$ increases linearly, the exposure time must decrease hyperbolically to deliver the same 1.5 mSv of ^{137}Cs (assuming that at any given time the air kerma rate remains constant):

$$(\dot{K}_{a,Cs} \leftrightarrow) (t \downarrow) (C_{K,d,Cs} \uparrow) = 1.5 \text{ mSv} \quad (A6)$$

As $C_{K,d,Cs}$ increases the calibration cards would be irradiated for a shorter time under the same air kerma

rate. This results in the cards receiving less radiation and yielding less light output when read. This shows up as a hyperbolic decrease in the numerator of Equation A1 which results in the decrease in the RCF discussed above.

The above result remains the same when considering a NIST traceable local source. To show this, first consider the steps the Naval Dosimetry Center takes to make a local ^{137}Cs source NIST traceable.

- (1) Irradiate calibration cards with 1.5 mSv of ^{137}Cs at NIST.
- (2) Read them in the TLD reader to obtain a value of nanocoulombs of light output per mSv received.
- (3) Expose the same cards with the local ^{137}Cs source for 50 s.
- (4) Read them in the reader to obtain a value of nanocoulombs of light output per second of exposure.
- (5) Divide the results from step 4 by step 2 to obtain a NIST traceable local source dose equivalent rate in units of mSv per second.

These steps are summarized by Equation A7:

$$\frac{\text{mSv}}{\text{s}} \text{ by local source} = \frac{\left(\frac{\text{Light output from local exposure}}{50 \text{ s}} \right)}{\left(\frac{\text{Light output from NIST Exposure}}{150 \text{ mSv}} \right)} \quad (A7)$$

The numerator of Equation A7 is not affected by changes in $C_{K,d,Cs}$. However, the denominator will decrease with increases in $C_{K,d,Cs}$ as explained previously. This has the effect of raising the dose equivalent rate of the local source as shown by Equation A8:

$$\frac{\text{mSv}}{\text{s}} \text{ by local source} = \frac{(\text{Light output from local exposure}) (150 \text{ mSv})}{(50 \text{ s}) (\text{Light output from NIST Exposure} \downarrow)} \Rightarrow \frac{\text{mSv}}{\text{s}} \uparrow \quad (A8)$$

Each subsequent time the local source is used to irradiate the calibration cards, for calibration of the reader, the higher rate will be applied so that the time to obtain 1.5 mSv is smaller than would have been with the older lower value of $C_{K,d,Cs}$. This means that the

Table A1. Predicted changes in the RCF with changes in $C_{K,d,Cs}$.

Table of results for DT648	RCF Channel 1 (nC.mSv ⁻¹)	RCF Channel 2 (nC.mSv ⁻¹)	RCF Channel 3 (nC.mSv ⁻¹)	RCF Channel 4 (nC.mSv ⁻¹)
Old average from July 1994	0.5779	0.6355	0.1907	0.4870
New predicted from Equation 4	0.5587	0.6145	0.1844	0.4709
New actual from August 1995	0.5613	0.6170	0.1815	0.4716
% error = (Predicted-Actual)/Actual × 100	-0.46%	-0.41%	1.6%	-0.15%

IMPACT OF ANSI STANDARD ON TLD PROCESSORS

calibration cards receive less total exposure due to the increase in $C_{K,d,C}$. When the cards are read, less light output is given, so that the RCF decreases as shown by Equation A1. This is the same result as previously obtained when the calibration cards were assumed to be irradiated at NIST.

REFERENCES

1. Schauer, D. A. and Zeman, G. H. *The Application of ICRU-39 Operational Dose Equivalent Quantities in Practical Dosimeter Calibrations*. Paper at the Annual Meeting of the Health Physics Society 35th Annual Meeting, Anaheim, CA (1990).
2. American National Standards Institute N13.11-1983. *Personnel Dosimetry Performance — Criteria for Testing*. ANSI N13.11 (1983).
3. Federal Register Notice (FRN), Nov 21 (1994).
4. NVLAP Laboratory Bulletin. *Dosimetry*, Vol II, No. 1, Effective Date: January (1995).
5. Soares, C. G. and Martin, P. R. *A Comprehensive Set of Conversion Coefficients for Photons*. In: Proc. Harshaw User's Group Meeting, Las Vegas, NV, 13-17 March 1995.
6. Health Physics Society N13.11-1993. *Personnel Dosimetry Performance — Criteria for Testing*. HPS N13.11 (1993).
7. Moscovitch, M. *Dose Algorithms for Personal Thermoluminescence Dosimetry*. Radiat. Prot. Dosim. **47**, 373-380 (1993).
8. Moscovitch, M. (Editorial) *Effective Algorithms*. Radiat. Prot. Dosim. **35**, 147-148 (1991).
9. Moscovitch, M., Velbeck, K. J. and Bencke, G. M. *Mixed Field Personnel Dosimetry Using a Nearly Tissue-Equivalent Multi-Element Thermoluminescent Dosimeter*. Radiat. Prot. Dosim. **34**, 145-148 (1990).
10. Devine, R. T., Moscovitch, M. and Blake, P. K. *The US Naval Dosimetry Center Thermoluminescent Dosimetry System*. Radiat. Prot. Dosim. **30**, 231-236 (1990).
11. Moscovitch, M., Tawil, R. A., Thompson, D. and Rhea, T. A. *Dose Calculation Algorithm of the Department of Energy Laboratory Accreditation Program*. In: Proc. 3rd Conf. on Radiation Protection and Dosimetry, Orlando. ORNL/TM-11882, pp. 60-68 (October 1991).
12. Moscovitch, M., Chamberlain, J. D. and Velbeck, K. J. *Dose Determination Algorithms for a Nearly Tissue Equivalent Multi-Element Thermoluminescent Dosimeter*. In: Proc. 2nd Conf. on Radiation Protection and Dosimetry, Orlando. ORNL/TM-10971, pp. 48-59 (October 1988).